Fate of Springtime Atmospheric Reactive Mercury: Concentrations and Deposition at Zeppelin, Svalbard

Stefan Osterwalder, Sarrah Dunham-Cheatham, Beatriz Ferreira Araujo, Olivier Magand, Jennie Thomas, Foteini Baladima, Katrine Aspmo Pfaffhuber, Torunn Berg, Lei Zhang, Jiaoyan Huang, et al.

HAL Id: hal-04482777

https://hal.univ-grenoble-alpes.fr/hal-04482777

Submitted on 4 Apr 2024

Fate of Springtime Atmospheric Reactive Mercury: Concentrations and Deposition at Zeppelin, Svalbard

Journal Article

Author(s):
Osterwalder, Stefan ; Dunham-Cheatham, Sarrah M.; Ferreira Araujo, Beatriz; Magand, Olivier; Thomas, Jennie L.; Baladima, Foteini; Pfaffhuber, Katrine Aspmo; Berg, Torunn; Zhang, Lei; Huang, Jiaoyan; Dommergue, Aurélien; Sonke, Jeroen E.; Sexauer Gustin, Mae

Fate of springtime atmospheric reactive mercury: Concentrations and deposition at Zeppelin, Svalbard

Stefan Osterwalder[1,2*], Sarrah M. Dunham-Cheatham[3], Beatriz Ferreira Araujo[4], Olivier Magand[1], Jennie L. Thomas[1], Foteini Baladima[1], Katrine Aspmo Pfaffhuber[5], Torunn Berg[6], Lei Zhang[7], Jiaoyan Huang[8], Aurélien Dommergue[1], Jeroen E. Sonke[4], Mae Sexauer Gustin[3]

[1] Institut des Géosciences de l'Environnement, Université Grenoble Alpes, CNRS, IRD, Grenoble INP, 460 Rue de la piscine, 38400 Saint-Martin-d'Hères, France

[2] Institute of Agricultural Sciences, ETH Zurich, Universitätstrasse 2, 8092 Zurich, Switzerland

[3] Department of Natural Resources and Environmental Sciences, University of Nevada, 1664 N. Virginia Street Reno, NV 89557, USA

[4] CNRS, IRD, CET, Université Paul Sabatier–Toulouse III, Observatoire Midi-Pyrénées 14, avenue Édouard Belin 31400 Toulouse, France

[5] Norwegian Institute for Air Research, Instituttveien 18, 2007 Kjeller, Norway.

[6] Department of Chemistry, Norwegian University of Science and Technology, Gløshaugen, 7491 Trondheim, Norway

[7] School of the Environment, Nanjing University, 163 Xianlin Avenue, Nanjing, Jiangsu 210023, China

[8] Sonoma Technology, 1450 N. McDowell Blvd., Suite 200, Petaluma, California 94954, USA

*corresponding author: stefan.osterwalder@usys.ethz.ch

KEYWORDS:

Aerohead, Arctic, Pollution, RMAS, Speciation, Thermal desorption

1   **Abstract**

2   Mid-latitude atmospheric elemental mercury (Hg) emissions undergo extensive oxidation to reactive

3   Hg (RM) compounds during Arctic polar sunrise, resulting in enhanced atmospheric deposition that

4   impacts Arctic marine wildlife and humans. It has been difficult to estimate RM dry deposition,

5   because RM concentrations, compounds, and their deposition velocities are ill-defined. Here we

6   investigate RM concentrations sampled with membrane-based methods, and find these to exceed

7   denuder-based RM detection by 5 times at the Zeppelin Observatory on Svalbard (March 26 – July 24,

8   2019). Measured dry deposition of GOM was about half of modeled RM deposition demonstrating

9   that particulate-bound Hg was an important component of dry deposition. Using thermal membrane

10   desorption RM chemistry was found to be dominated by Hg–Cl/Br (51%) and Hg–N (45%)

11   compounds. Back trajectory analysis indicated that Hg–Br/Cl compounds were predominantly

12   advected from within the marine boundary layer (sea ice exposure), while Hg–N originated from the

13   free troposphere. Weekly average RM compound-specific dry deposition velocities ranged from 0.12

14   to 0.49 cm s^{-1}, with a net RM dry deposition of 1.9 µg m^{-2} (1.5 – 2.5 µg m^{-2}; 95% confidence interval),

15   that exceeds the mean annual Hg wet deposition flux in Svalbard. Overall, we find that springtime

16   atmospheric RM deposition has been underestimated in the Arctic marine environment.

SYNOPSIS:

Atmospheric reactive mercury measurements at Svalbard demonstrate elevated deposition to Arctic ecosystems (5.6-times), and input of Hg-N and halogenated compounds.

1. Introduction

Mercury (Hg) pollution in the Arctic is of concern, because indigenous people rely heavily on marine-based diets that expose them to neurotoxic methylmercury[1,2]. Globally, the toxic burden of anthropogenic Hg pollution for human and ecosystem health is accepted by policy makers, and has resulted in the UNEP Minamata Convention that aims to reduce human and ecosystem exposure to Hg[3]. However, to evaluate the effectiveness of the Convention we must improve our understanding on how Hg cycles between air, land, water, ice, and snow, especially in vulnerable ecosystems, such as the Arctic[4]. The uncertainty in estimates of atmospheric Hg deposition as gaseous elemental Hg (GEM), gaseous oxidized Hg (GOM), or as particulate-bound Hg (PBM) to the Arctic Ocean is illustrated by a comparison of two global numerical Hg models. The GEOS-Chem model[4] suggested an atmospheric Hg input to the Arctic Ocean of 76 Mg yr^{-1}, while the GRAHM model estimated 108 Mg yr^{-1} [5].

The discovery of coastal springtime atmospheric Hg depletion events (AMDEs) in 1995 indicated that reactive Hg (RM = GOM + PBM) dry deposition was an important pathway for atmospheric Hg inputs to Arctic marine ecosystems[6]. Subsequent studies suggested that during AMDEs about 100 Mg RM yr^{-1} was deposited to Arctic snow and ice[7,8]. Oxidation of GEM to GOM during AMDEs is primarily induced by photochemical activation of sea ice-derived halogen compounds[8,9]. In particular, bromine oxide and atomic bromine radicals (BrOx, BrO, Br•) lead to the destruction of ozone (O_3) and oxidation of GEM, with subsequent depletion of both GEM and O_3 in the Arctic atmosphere during polar sunrise[10,11]. Most recently, Obrist et al.[12] found that RM dry deposition to coastal Arctic tundra was substantial during springtime AMDEs, depositing 0.8 – 2.8 µg m^{-2} yr^{-1}. Dry deposition of RM during AMDEs results in higher total Hg concentrations in snow[13,14] that can be followed by re-emission of Hg^0 after photo-reduction[2,15,16]. Approximately 90% of the total Hg in snow can be re-emitted back to the atmosphere after AMDEs[1].

To assess the total input of Hg to Arctic ecosystems during AMDEs, it is crucial to improve RM dry deposition estimates. This could be done by measuring ambient RM concentrations and applying the values in dry deposition models or identifying RM compounds in ambient air and applying compound-specific deposition velocity calculations based on local meteorological data. The spatial resolution of Arctic RM measurements is limited, and the widely used measurement technique to quantify atmospheric Hg (Tekran® speciation system [Tekran® 2537/1130/1135]; Tekran® Instrument Corp., Ontario, Canada) has been demonstrated to underestimate RM by a factor of 2 to 13 in the planetary boundary layer[17-24], and by a factor of 1.6 in the free troposphere[25]. Other studies suggest measurement artefacts for PBM are generated by temperature and collection time[26-28]. Selective collection and analysis of particles smaller than 2.5 µm diameter with the Tekran® also raises the question of the possible underestimation of PBM concentrations[29] particularly in oceanic environments where the RM compounds are dominantly associated with larger (2 – 10 µm) marine aerosols[30,31].

53 The University of Nevada, Reno – Reactive Mercury Active System 2.0 (RMAS), with cation
54 exchange membranes (CEM) and nylon membranes[32], in combination with a down-facing
55 aerodynamic sampler housing that also uses CEMs (Aerohead sampler)[33,34], have been shown to
56 improve RM concentration measurements, and GOM and RM dry deposition estimates, respectively,
57 relative to the Tekran® 2537/1130/1135 system [35]. These measurement methods have never been
58 applied in the Arctic, though they are necessary since a low bias in RM deposition would lead to
59 underestimation of Hg transfer from the atmosphere to marine and terrestrial ecosystems during
60 AMDEs. Using the RMAS, the chemistry of RM compounds can be suggested using thermal
61 desorption of nylon membranes and subsequent peak deconvolution[20,21,32,36]. This methodology allows
62 for understanding if specific compounds namely HgO, Hg-Br/Cl (e.g. $HgBr_2$, $HgCl_2$), Hg-nitrogen
63 (e.g., $Hg(NO_3)_2$), and Hg-sulfur (e.g., $HgSO_4$), as well as some organic-bound compounds (e.g.,
64 MeHg)[24] are present. Knowledge about the chemistry of RM improved local estimates of RM
65 deposition at a coastal research site in Florida, USA[36]. Estimates of dry deposition were based on
66 compound-specific deposition velocity calculations using a multiple resistance model that was
67 developed by Zhang et al.[37] and modified by Lyman et al.[33].

68 Explaining the bias in atmospheric RM concentration among different measurement methods, in
69 combination with better identification of chemical compounds of RM, has been identified as a top
70 priority task to improve the determination of RM dry deposition from local to global scales[18]. Here we
71 present a procedure to determine RM compound-specific dry deposition velocities in order to calculate
72 springtime RM dry deposition in the Ny-Ålesund area on Svalbard. The goals of the study were to: 1)
73 intercompare RM concentrations using automated (Tekran®) and manual methods (RMAS); 2)
74 identify RM compounds by thermal desorption procedures; 3) investigate the source of RM
75 compounds using back-trajectory analysis; and 4) calculate RM compound-specific dry deposition
76 velocities and compare them with dry deposition measurements made by the Aerohead sampler. The
77 incorporation of new observations of RM concentration, chemistry and compound-specific dry
78 deposition velocities is a necessary intermediate step toward substantially improving numerical
79 models of Hg cycling in the Arctic.

2. Material and Methods

2.1 Location and sampling

Air measurements were carried out from March 26 (11:00) to July 24 (08:00), 2019 at the Zeppelin Observatory (Zeppelin), located on Svalbard in the Norwegian Arctic. The atmospheric research and monitoring station was located on Zeppelin Mountain at 474 m a.s.l. (78.90°N, 11.88°E). The observatory was situated far from major air pollution sources, and thus, was within an undisturbed Arctic environment. A steep downhill slope faced north towards the research village of Ny-Ålesund, a small settlement with 35 to 185 inhabitants at 2 km from the sampling site. The station was operated by the Norwegian Institute for Air Research (NILU) in close collaboration with the Norwegian Polar Institute (NPI). Air inlets for all air Hg measurements were installed 3 m above ground in close proximity to one another, facing downward and toward the predominant wind direction (ESE). Automated atmospheric Hg measurements were carried out by Norwegian University of Science and Technology (NTNU) in collaboration with NILU; manual sampling for RM analyzes was performed by NPI staff. Previous analysis of automated atmospheric Hg and snow Hg measurements at Zeppelin were reported by Dommergue et al.[13], Berg et al.[38-40], Aspmo et al.[41], Gauchard et al.[42], Sprovieri et al.[43,44], Sommar et al.[45], Ferrari et al.[46], Steen et al.[47], and Angot et al.[48].

2.2 Automated GEM and RM measurements

During the campaign, a Tekran® measured GEM, GOM, and PBM continuously following methods briefly described in section S1 and detailed in Landis et al.[49]. The only deviation from the standard operation procedures[50,51] was calculating GOM with the flush blank concentrations added to the GOM measurement; this was done because adding the Tekran® flush blank to RM (GOM + PBM) measurements resulted in a good agreement with manual RM measurements using polyethersulfone membranes at the high altitude Pic du Midi Observatory[25].

2.3 Manual RM measurements

Three different sorption surface materials were used to sample RM. Polyethersulfone membrane (PES, 47 mm diameter, 0.45 μm pore size; Millipore) were previously applied[25,52] and showed a similar sorption capacity and background Hg contents to CEM[53]. The PES and CEM (PES backbone that has been proprietarily treated, 47 mm diameter, 0.8 μm pore size; Mustang-S, Pall Corporation) were applied extensively in recent studies (e.g., Gustin et al.[19]; Maruszczak et al.[25]; Luippold et al.[32], Miller et al.[54]) and were deemed the preferable material for quantitative RM measurements due to the high RM sorption efficiency[53]. Nylon membranes (47 mm diameter, 0.2 μm pore size; Sartorius Stedium) were used to determine the chemistry of RM using thermal desorption procedures[19,24]. The chemistry of the RM compounds captured on the nylon membranes was determined by comparing membrane Hg desorption profiles from Svalbard with those developed for standard Hg compounds (see section 2.4 also).

2.3.1 PES measurements

The PES sampling configuration captured RM in ambient air by pumping at 1 L min^{-1} (Membrane vacuum pump, KNF) through a one-stage outdoor filter pack protected from snow fall. The airflow was regulated by a ball flow meter (Fisher Scientific) and quantified with a digital volume meter (Siargo Ltd.). The flow was regularly checked with a Bios Defender calibration unit and considered stable throughout the campaign. In the laboratory, the RM content on the PES after digestion was determined using a Brooks Rand Model III cold vapor atomic fluorescence spectrometer (CVAFS). The method detection limit (MDL) was 5 pg Hg[25]. Details on RM analysis are described in section S2 and a data overview is given in section S3. In total, eight blank membranes were collected from the jars that housed the PES prior to deployment of the new samples. The mean Hg content on PES blanks was 13 ± 8 pg (1σ, n = 8). The limit of detection (LOD) was 25 pg (3σ of blank). The lowest RM on PES was 333 pg, collected from June 4 to June 11, 2019. The blank percentage compared to the median RM was 2% (ranged from 1% to 6%) and all samples were above the LOD.

2.3.2 RMAS membrane total Hg measurements

The RMAS was used to collect RM on CEM and nylon membranes. The sampling procedures for CEM and nylon membranes and their blank treatments were identical. Previous studies showed that nylon membranes did not collect all ambient compounds with the same efficiency as CEMs[19,53], but that the RM chemistry was in good agreement with measurements of anions (e.g., Cl$^-$, Br$^-$, NO$_3$$^-$)[24], and that RM compounds sorbed to the membrane did not transform during storage and shipment[53]. For RM sampling, ambient air was drawn through 6 sampling ports (n = 3 CEM, n = 3 nylon) at a flow rate of 1.7 ± 0.2 L min^{-1}. The downstream membranes in the two-stage filter holders allowed for the capture of Hg that passed through the upstream membrane. A detailed description of the RMAS can be found in Luippold et al.[24]. Triplicate blank CEM and nylon membranes were collected from the same jars as those that held the sample membranes. CEM and downstream nylon membranes were digested and analyzed using CVAFS following EPA Method 1631, and upstream nylon membranes are thermally desorbed (sections 2.4, S2). The mean of the triplicate CEM blanks, collected weekly at the start of each deployment, was 38 ± 13 pg (1σ, n = 17), and the mean nylon membrane blank Hg content was 14 ± 7 pg (1σ, n = 17). All CEM samples were above the LOD of 38 pg (3σ of blank); the LOD was less than 5% of the median RM (785 pg). Median CEM breakthrough for all samples was 8% (n = 17). The nylon membrane LOD was 20 pg (3σ of blank); the two last samples of the campaign (harvested on July 17 and 24, 2019) were below the LOD. The mean breakthrough on the nylon membrane was 2% (1σ, n = 15), excluding the samples below the LOD.

2.4 RM compounds

Upstream nylon membranes were thermally desorbed to characterize and quantify RM compounds. The thermal desorption profiles for different RM compounds (Section S4) were compared to pure GOM compounds for which profiles have been developed, including HgO, HgBr$_2$, HgCl$_2$, HgN$_2$O$_6$,

151   HgSO$_4$, and elemental Hg, as well as methylmercury chloride directly added to membranes[20,21,36].

152   Thermal desorption profiles have been used to identify Hg compounds not only in ambient air but in

153   other matrices. Exemplarily, Biester and Scholz[55] developed profiles for solids that have peaks at

154   similar locations as ours for similar compounds.

155   Individual RM compounds were identified from peak deconvolution of thermal desorption

156   profiles[19,20,24,32]. Each profile was considered to follow a Gaussian distribution (Section S3) and was

157   deconvoluted based on the curve fitting function in MATLAB v. 2018a. Peak temperature ranges were

158   defined for different compounds using an improved calibration system: 80–85 °C for [-O], 90–110 °C

159   for [-Br/Cl], 125–135 °C for [-N], 150–155 °C for [-S], and 180–190 °C for methylmercury (MeHg) or

160   generally organic Hg compounds[24,32]. To quantify the RM compounds on each nylon membrane, the

161   integral of the area beneath each Gaussian peak was calculated (pg·m^{-3}·°C). The relative contribution

162   of each RM compound was calculated based on the integrated peak area. The percentage of the

163   compounds was determined by dividing the concentration of the identified compound using thermal

164   desorption data, specifically the area under the curve, by the total amount of RM measured. RM

165   compound contribution collected on each nylon membrane was determined weekly based on the peak

166   deconvolution analysis. For details on the thermal desorption and peak deconvolution procedures, see

167   Luippold et al.[32].

2.5 Back trajectory modeling

169   The Hybrid Single-Particle Lagrangian Integrated Trajectory model (HYSPLIT, v. 4.2.0), developed

170   by NOAA[56], was driven with 3-hourly meteorological input data from the Global Data Analysis

171   System (GDAS; 1° latitude-longitude 360 by 181 grid) to identify the potential source regions of RM

172   compounds. The model was run in backward mode for 10 days every 2 hours throughout the CEM and

173   nylon membrane sampling periods at Zeppelin (474 m a.s.l.). In total, ~84 backward trajectories were

174   calculated for each sampling period. The spatial (horizontal and vertical) residence time of the air

175   masses were calculated. The back trajectory model results were combined with five major surface

176   categories – land (no snow cover), open water, permanent ice/snow, sea ice, and snow on land,

177   determined using ESRI ArcGIS Pro (v. 10.6) – to provide the time series of percent surface exposure

178   of particles along trajectories. Moreover, the percent of particles along trajectories that reside within

179   the boundary layer (BL) and in the free troposphere (FT) was analyzed. Details on generation of

180   surface maps and back trajectory statistics are given in section S5.

2.6 GOM/RM dry deposition

2.6.1 Dry deposition measurements

183 Three passive Aerohead samplers were deployed to measure GOM dry deposition[33,34] next to the inlets

184   for the automated and manual RM samplers. GOM was collected on CEM (127 mm diameter, 0.8 μm

185   pore size; Mustang-S, Pall Corporation) on a weekly basis. After each deployment, the three CEM and

186   two non-deployed blanks were collected. The samples were stored in 50 mL centrifuge tubes in

187   double-zipper bags at -20 °C. In the laboratory, the membranes were digested and analyzed identically

188   to the CEM and nylon from the RMAS. Dry deposition of RM was calculated following Lyman et al.

189   [34]:

190     $$D = \frac{\left[\frac{S-B}{A}\right]}{T},$$ (1)

191   where D is the deposition rate in ng m^{-2} h^{-1}, S is the mass of Hg on the membrane (ng), B is the mass

192   of Hg on the method blanks (ng), A is the surface area of the membrane (0.0104 m^2), and T is the

193   deployment duration (h). The mean of all Aerohead CEM blanks was 166 ± 112 pg (1σ, n = 35). The

194   RM dry deposition MDL for a weekly deployment was 0.29 ng m^{-2} h^{-1} (blank + 3σ). Uncertainty in the

195   GOM dry deposition measurements originiates from the fact that we measure deposition on an

196   artificial surface and not on snow, ice or tundra vegetation directly, where GOM can be reduced and

197   subsequently re-emitted to the atmosphere. The surface of the CEM provides physical means for

198   understanding temporal changes of GOM dry deposition[34].

199   **2.6.2 Dry deposition modeling**

200   Weekly dry deposition of RM was estimated in a three step procedure. First, we determined the

201   individual RM compounds (Hg(OH)$_2$, HgBr$_2$/HgCl$_2$, HgN$_2$O$_6$, HgSO$_4$, MeHg) using thermal

202   desorption and peak deconvolution procedures (Section 2.4). Second, we calculated the RM

203   compound specific dry deposition velocity using a multi-resistance model[37]. The basic source code of

204   the multi-resistance model was described in Lyman et al.[33] and was subsequently applied by Huang et

205   al.[36]. Here the code was modified according to the description in section S6, and is publicly accessible

206   (https://github.com/JiaoyanHuang/Dry_Depo_multi_res_model). The meteorological model input

207   parameters were derived from hourly ERA5 data, the fifth generation ECMWF atmospheric reanalysis

208   of the global climate[57]. The meteorological data were representative for a 31 km grid covering the area

209   around Zeppelin. Snow depth was determined at two measurement stations representing a lower and

210   upper limit of snow depth in the area. The first station, representing low snow depth, was located on a

211   measurement field just south of the Ny-Ålesund village; the second station, Bayelva, was located

212   about 3 km outside the village and represented the upper limit of snow depth[58]. Third, we multiplied

213   the RM compound specific dry deposition velocities (calculated by the model) with the relative

214   percentage of the RM compound concentrations measured by the Tekran® or from CEM analysis.

215   **2.7 Uncertainty in RM dry deposition modeling**

216   The uncertainty of the modeled RM dry deposition was assessed using the Monte Carlo simulation

217   approach (Crystal Ball®) and is reported as the 95% confidence interval of 10,000 simulations. The

218   probability distributions of the key input parameters for the model was obtained using the "BatchFit"

219   function in Crystal Ball® based on the dataset for each sampling period. Normal distribution and log-

220   normal distribution were chosen for distribution fitting, and the *p* values for the significance levels of

221   the fitted distributions were all < 0.05. The uncertainty analysis, however, does not include the issues

222   of 1) lower sorption efficiency (ca. 50%) of RM on nylon membranes compared to CEMs and 2) that

223   during peak deconvolution mixed compounds, e.g. $HgBrNO_3$, are not well-defined. In order to

224   minimize these uncertainties, the nylon membranes were not used as a quantitative sorption surface

225   but for RM compound analysis only. Several studies have confirmed, that nylon membranes sorbed

226   Hg-Br and Hg-Cl compounds linearly with increasing concentrations (under ambient and laboratory

227   conditions)[22,53], and these compounds were neither lost nor transformed RM during sampling and

228   storage[53]. However, CEM collected systematically higher concentrations of $HgBr_2$, $HgCl_2$, and a HgO

229   compound[21]. More recent work has demonstrated that the nylon membranes do not effectively collect

230   Hg-N compounds[20]. We are learning incrementally about the use of membrane for identifying the

231   chemistry of the compounds. Thermal desorption and peak deconvolution procedure introduces

232   uncertainty, because there are only a limited number of RM compounds for which calibration profiles

233   can be developed and currently the desorption profiles are broad. However, comparing the chemistry

234   of the compounds to oxidants measured or expected in the air for a variety of locations, as well as ion

235   chromatography measurement of ions on the nylon membranes, supports the RM chemistry observed.

236   For example, in Hawaii halogenated compounds were dominant, while in Nevada adjacent to a high

237   way N-S-O Hg compounds were present, and in a forested area in Maryland organic compounds were

238   measured[24]. This indicates that we are effectively getting at the compounds in general, although we do

239   not know the exact chemistry. More work needs to be done to quantify the chemistry and develop

240   surfaces that are better at retaining compounds.

241   **2.8 Auxiliary variables**

242   Meteorological parameters from Zeppelin, including air temperature, wind speed, wind direction,

243   relative humidity, and atmospheric pressure, were provided with an hourly resolution by NILU.

244   Hourly means of tropospheric O_3 concentrations were measured by NILU using a UV absorption

245   spectrometer (API 400A). Hourly means of particulate matter concentrations ($PM_{2.5}$, PM_{10}, and

246   PM_{total}) were derived from a FIDAS® 200S instrument (Palas GmbH, Germany) operated by

247   Stockholm University (SU). Daily means of particulate and gaseous nitrogen compounds (HNO_3/NO_3^-,

248   NH_4^+/NH_3) were collected on a three stage filter pack and analyzed using a Thermo Scientific Dionex

249   Integrion HPIC System equipped with a Dionex AS9-column[59] and made available by NILU.

250   **3. Results and Discussion**

251   **3.1 Quantification of atmospheric Hg using the Tekran® system**

252   The mean GEM $\pm$ 1σ concentration measured between March 26 and July 27, 2019 was 1.36 $\pm$ 0.4 ng

253   m^{-3} (Figure 1a). During that period, nine distinct AMDEs were identified, with eight observed in April

254   and May and one in early June. The occurence of an AMDE was defined when GEM decreased below

255   1 ng m^{-3} [41] and the O_3 concentration dropped below the 5th percentile (33 µg m^{-3}). An AMDE starts

256   when the concentration of GEM sharply decreases and ends when GEM increases again to average

257   concentrations. Due to AMDEs, GEM concentrations in the Arctic are typically the lowest in April

258 and May. From 2000 – 2009[39] and 2011 – 2015[48], 86% and 75%, respectively, of annual observed

259 AMDEs occurred during the April and May time period. Due to the influence of AMDEs during the

260 sampling campaign, the mean GEM concentration during the campaign (1.36 ng m^{-3}) was lower than

261 the annual mean of 1.54 ± 0.3 ng m^{-3} measured between 2000 and 2009[39] and annual means ranging

262 from 1.47 – 1.51 ng m^{-3} between 2011 and 2015[48]. In summer, GEM increases due to re-emission of

263 previously deposited Hg to surfaces and re-emission of surface Arctic Ocean dissolved Hg^0 [60-62].
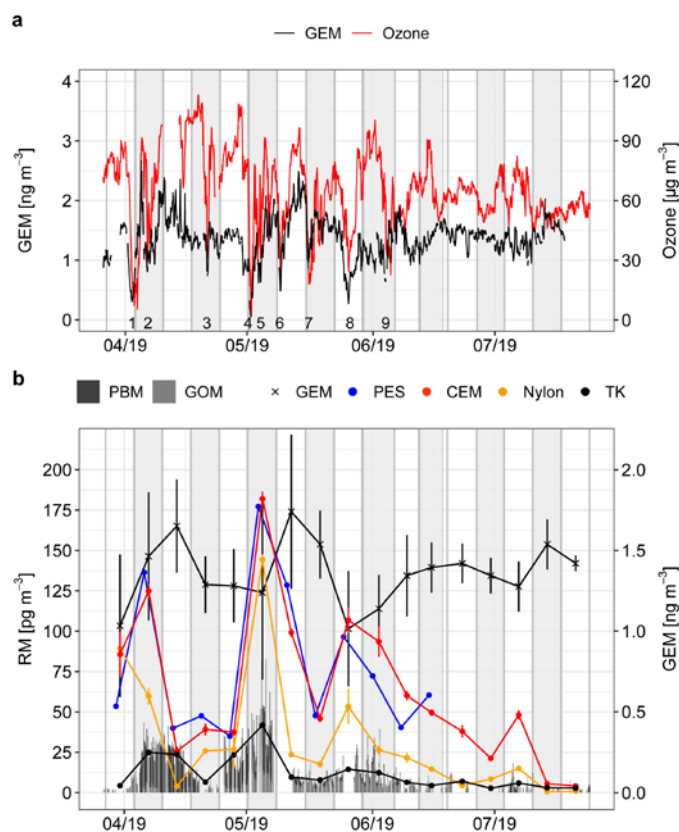

Figure 1: Time series of atmospheric Hg species and O$_3$ from March 26 to July 27, 2019. (a) GEM (black line) and O$_3$ (red line) concentrations are displayed as hourly means. AMDEs are indicated with numbers 1 to 9. (b) Mean concentration of GEM (black cross), RM on PES (blue dots), RM on CEM (red dots), and RM on nylon membranes (orange dots). RM from Tekran® (TK) measurements (black dots), as PBM and GOM measurements (gray bars), are also displayed. Error bars represent 1σ and are indicated where n ≥ 3. PES, CEM, and nylon membranes were deployed for one week. Sampling periods for CEM and nylon membranes are indicated with alternate white and gray backgrounds. The weekly PES sampling was offset from CEM and nylon membrane by one day.

264 Automated Tekran® measurements of RM (GOM+PBM) for the whole sampling campaign were in

265 the range of 2.6 – 13.1 pg m^{-3} for GOM and 2.1 – 29.9 pg m^{-3} for PBM (10th and 90th percentiles). The

266 mean Tekran® RM concentration (RM$_{TK}$) was 14.6 ± 12.7 pg m^{-3}, and the values spanned from below

267 the MDL to 82.6 pg m^{-3} (Figure 1b). During AMDEs, GOM and PBM concentrations were 9.6 and

268 20.5 pg m^{-3}, on average, and elevated by 42% and 54%, respectively, compared to the entire campaign

269 average. These values were at the lower end compared to those measured at Zeppelin during AMDEs

270 in 2003[41] and in 2007-2008[47]. Overall, RM$_{TK}$ was < 43.5 pg m^{-3} (90th percentile) during AMDEs and

271 lower (< 30.8 pg m^{-3}, 90th percentile) during the entire campaign.

3.2 Quantification of RM using manual methods

Mean RM concentration sampled on CEM (RM_{CEM}) was 63 ± 45 pg m^{-3} (Section S3). The highest concentrations were found between May 1 and May 8 (182 pg m^{-3}) and lowest at the end of the campaign from July 17 to July 24 (4 pg m^{-3}). The large variation among samples was due to the occurrence of AMDEs until the beginning of June (Figure 1b). Thereafter, RM_{CEM} tended to decrease, with one exception from July 3 to July 10 when RM_{CEM} was 48 pg m^{-3}. The RM concentration on PES (RM_{PES}) was sampled until June 18, 2019 and was similar to RM_{CEM} even though the PES were replaced one day in advance compared to CEM (slope = 0.91, $r^2 = 0.86$; Figure S1a). The mean RM_{PES} was 78 ± 46 pg m^{-3}, similar to mean RM_{CEM} concentrations for the same period to within 2% (March 26 – June 18). The good agreement between the CEM and PES materials was previously demonstrated by Dunham-Cheatham et al.[53], showing no significant difference between the two materials ($\alpha = 0.05$). In concert with that study, the nylon membranes in this study were less efficient at capturing RM.

The mean RM concentration on nylon membranes (RM_{Nylon}) was 32 ± 37 pg m^{-3}. The nylon membrane recovery was 50% (range from 12 to 104%) of the RM sorbed on CEM (Figure 1b). The lower RM content on nylon membranes was likely due to the different sorption efficiency of varying RM compounds to this material[19,20,24,36]. Despite the difference in captured RM, the relationship between RM_{CEM} and RM_{Nylon} was fairly constant ($r^2 = 0.75$, $p < 0.05$, section S3). This supports the conclusions from previous studies that nylon membranes are not suitable for quantitative RM concentrations, but are suitable for thermal desorption analysis to identify RM compounds[19,53].

Weekly mean RM_{CEM} and RM_{PES} were up to 19 times and 22 times higher compared to RM_{TK}, respectively (Figure S1b). On average, the RM_{CEM} was 5.3 times and RM_{PES} 5.2 times higher than RM_{TK} based on weekly averages (11.8 ± 10.4 pg m^{-3}). Tekran® RM measurements were calculated as the sum of GOM and PBM concentrations and the amount of Hg released during the three 5-min flush cycles (flush$_{TK1-3}$). The discrepancy between RM on membranes and RM_{TK} agrees with recently performed comparisons, where RM on membranes was 2 to 13 times greater[17,18,20-22]. However, we would like to point out that the impactor on the Tekran® removes particles with aerodynamic diameters larger than 2.5 µm while the membrane-based systems might also capture particles > 2.5 µm. The mean $PM_{2.5}$ concentration (0.97 µg m^{-3}) was only 30% of the total mean PM concentration (3.29 µg m^{-3}) measured during our campaign. Thus, RM_{TK} tend to be lower compared to membrane-based systems due to the lower efficiency of GOM collection[63] and due to the exclusion of large PBM (> 2.5 µm) from analysis. More multi-season RM_{CEM} and RM_{PES} timeseries at multiple Arctic sites are necessary to derive robust correlations with automated measurements and to potentially correct previous Tekran® RM data.

3.3 Compounds of RM

Thermal desorption and peak deconvolution revealed the composition of RM species that were retained on the nylon membranes (section S4). The weekly mean RM_{Nylon} ranged from 1 to 144 pg m^{-3}

(Figure 2a). The dominant RM compounds sampled over the course of the campaign were Hg-Br/Cl and Hg-N, that accounted for 51% and 45%, respectively, of the total RM on nylon membranes (Figure 2b). Organic-based Hg compounds (e.g. MeHg) contributed 2% to the overall RM concentration. Sulfur compounds (Hg-S) accounted also for 2% while the contribution of oxide compounds (HgO) was < 1%. The relative contribution of the RM compounds was calculated each week throughout the campaign (Figure 2c). The Hg–Br/Cl compounds indicate reactions of GEM with halogens (Cl, Cl_2, Br, Br_2) within the atmospheric BL[7], where Br• is regarded as one of the primary first-step atmospheric oxidants to produce RM intermediates such as $Hg^I Br$[11,64]. The occurrence of Hg–N compounds depends on several different factors, such as N emission sources or atmospheric redox processes occurring between the source and receptor site[65-67]. Atmospheric NO_2 radicals are also considered to be the dominant second-step oxidant transforming $Hg^I Br$ to $Hg^{II} BrONO$ in the free troposphere[64,68]. During the first sampling deployment week, RM was composed of 34% Hg–Br/Cl and 58% Hg–N compounds, but in contrast, during week two, 68% Hg–Br/Cl and 32% Hg–N were detected. During week 6, when two AMDEs occurred and the largest RM concentrations were measured (182 pg m^{-3}), Hg–Br/Cl and Hg–N contributed similar parts to total RM (58% and 42%, respectively). During weeks seven and eight, the dominant RM compound on the nylon membranes changed from Hg–N (70%) to Hg–Br/Cl (89%). To explain differences in chemical composition, we investigated the role of air mass exposure on the dominant RM compounds, Hg–Br/Cl (51%) and Hg–N (45%), along the air mass back trajectory.
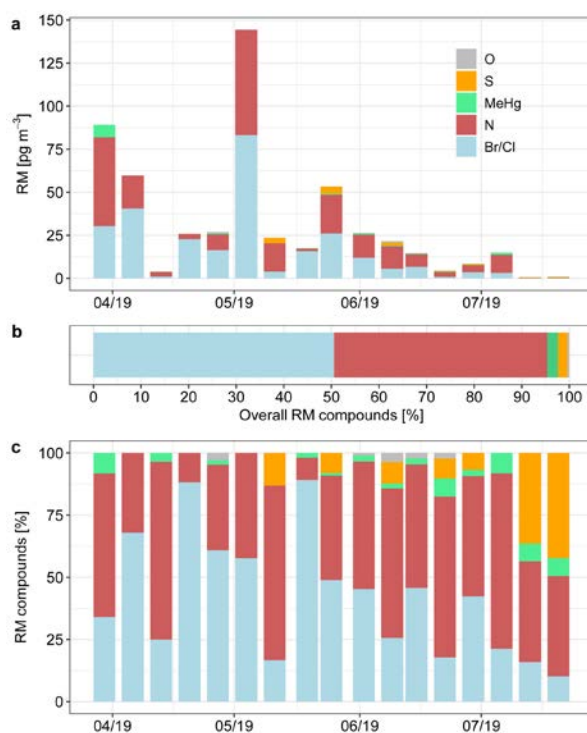

Figure 2: RM compounds determined from March 27 until July 24, 2019. (a) The RM concentration on the nylon membrane from the RMAS for a mixture of RM compounds identified by thermal desorption and peak deconvolution. The frequency distribution of RM compounds, in %, is given (b) for the entire campaign (mean) and (c) for each sampling event.

3.4 Origin of RM

328 To investigate if atmospheric conditions influence the RM compounds, the relationship between the

329 trajectories within the BL and in the FT was analyzed. The percentage of time the trajectories arriving

330 at Zeppelin resided in the BL ranged from 7% to 50% (Figure 3a). There was a significant correlation

331 between the percentage of time the trajectories were within the BL and the determined percentage of

332 Hg–Br/Cl compounds ($r^2 = 0.4$, $p < 0.05$). The relationship became even stronger during periods when

333 AMDEs occurred ($r^2 = 0.7$, $p < 0.05$) (Figure 3b). During the same period, Hg–N compounds occurred

334 more frequently when the advected air mass originated from the FT ($r^2 = 0.7$, $p < 0.05$) (Figure 3c).

335 This indicates that air masses enriched in Hg–Br/Cl were in contact with the surface for longer periods

336 compared to air masses enriched in Hg–N, that were originating predominantly in the FT.

337 Air masses arriving at Zeppelin were mainly exposed to sea ice and open water (Figure 3d). The RM

338 concentrations increased when air masses were exposed to sea ice ($r^2 = 0.32$, $p < 0.05$) or land covered

339 by snow ($r^2 = 0.36$, $p < 0.05$) (Figure 3e). Lower RM concentrations were measured when air masses

340 were exposed to open water ($r^2 = 0.43$, $p < 0.05$) (Figure 3f). The positive relationship between Hg–

341 BrCl and the time the air mass passed over sea ice ($p = 0.06$, Figure S4) further corroborates that sea

342 ice and snow on sea ice are the main source of reactive halogen species in the Arctic that oxidize

343 GEM. This can occur via one of two mechanisms, activation from snow on sea ice (surface snow

344 source)[69] or lofted salty snow particles that form sea salt aerosols within the BL (blowing snow

345 particle source)[70,71].Though Hg–Br and Hg–Cl compounds are indistinguishable with our methods, all

346 reactive halogen species in the atmosphere are produced from similar sources, i.e., snow on sea ice and

347 BL aerosols[72-74]. In the atmosphere, both Br• and Cl• react with O_3 to form halogen oxides[75,76]; both

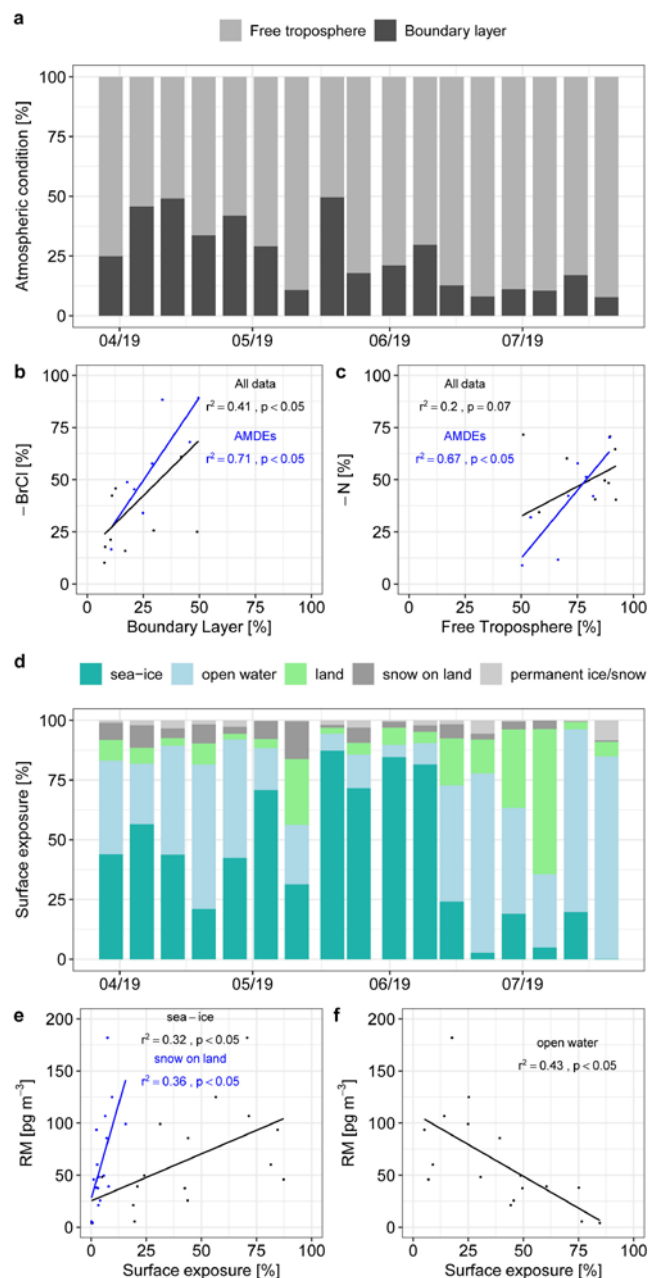348 halogen radicals and halogen oxides lead to the oxidation of GEM to RM[10].

Figure 3: HYSPLIT simulation of air mass trajectory residence time in the atmosphere and exposure to surfaces. (a) Percentage of time the trajectories were in the boundary layer (BL) and free troposphere (FT) for each of the 17 deployment periods. Linear correlation during the entire campaign and during weeks when AMDEs occurred (b) between Hg-Br/Cl and residence time in the BL and (c) Hg-N and residence time in the FT. (d) Surface exposure of trajectories to the 5 major surface categories: sea ice, open water, land (no snow), snow covered land, and permanent ice and snow. Linear correlation between (e) RM_{CEM} and exposure to sea ice and snow covered land, and between (f) RM_{CEM} and exposure to open water.

349 A weak positive relationship between Hg–N and the time the air mass passed over land without snow

350 cover ($r^2 = 0.2$, p = 0.06, Figure S4) indicated an anthropogenic source of N compounds (i.e. NO_2)

351 from more densely populated areas further south, or more specifically, springtime transport of plumes

352 from Asian industries or Siberian wildfires[77]. Emitted NO_2 leads to enhanced GEM oxidation and

353 increased Hg-N concentrations downwind. Though more data are required (multi-seasonal sampling)

354 to establish significant relationships between RM compounds and exposure time of air masses to

14

different surface types, our conclusions are well illustrated by comparing surface exposure during weeks seven and eight. A maximum of Hg–N compounds was measured during week 7 (70% of total RM), when exposure time of air masses over land (43%) and the residence time in the FT (89%) were long. Back trajectory analysis indicated that the air moved mainly from Fennoscandia (17%) and Siberia (74%) over the eastern Arctic Ocean to Zeppelin (Figure S5g). The Siberian air mass originated from areas where wildfires were ubiquitous between May 8 and May 15, 2019 (https://earthdata.nasa.gov/earth-observation-data/near-real-time/firms). The mean BL height measured along the air mass trajectories was 277 m a.s.l and was elevated compared to week 8 (87 m a.s.l). In week 8, Hg–Br/Cl was the dominant RM compound (89%) and air masses passed predominantly over sea ice (87%) from areas east of Zemlya Georga and northwest of Svalbard to Zeppelin (Figure S5h). The residence time of the air mass in the BL was 50%, which corresponded to the longest residence time in the BL among all weeks of sampling (Figure 3a). Thus, the comparatively long residence time of air masses within the BL over the sea ice-covered Arctic Ocean constituted the main source region of Hg–Br/Cl arriving at Zeppelin.

3.5 Dry deposition measurements and modeling

Mean local GOM dry deposition at Zeppelin measured by Aerohead samplers was 0.35 ng m^{-2} h^{-1}, and weekly averages ranged from below the MDL to 1.47 ng m^{-2} h^{-1} (Figure 4). Measurements of GOM dry deposition in 9 out of 17 weeks were above the MDL (0.29 ng m^{-2} h^{-1}). The cumulative Aerohead GOM dry deposition measured from March 27 to July 24, 2019 was 1 µg m^{-2}, with a 95% confidence interval ranging from 0.74 to 1.25 µg m^{-2} (Figure 4). Dry deposition of GOM measured by Aerohead samplers was negligible (< 0.1% of the cumulative flux) during the last 5 weeks of measurements (June 19 to July 27, 2019). During weeks 3 and 4, there was less than 1 pg GOM measured on the Aerohead CEM, in contrast to 795 pg analyzed on the CEMs from RMAS indicating the importance of particulate-bound Hg. During weeks 5 and 9, measured GOM dry deposition exceeded the modeled RM dry deposition by 38% and 43%, respectively. A comparison of meteorological and chemical variables during these weeks with the preceding and following weeks indicated no unusual conditions. It could be a compound was present that was sticking to the open-faced membranes in the Aeroheads, but not making its way into the filter packs holding membranes in the RMAS or the compound had a higher deposition velocity than other compounds. This would be true for HgO that once formed is thought to become a particle and rapidly deposit to surfaces[78]. Thus, understanding reactions forming and the chemistry of compounds of GOM/RM is greatly needed.

The cumulative modeled dry deposition of RM, based on RM compound-specific dry deposition velocities and RM$_{TK}$, was 0.33 µg m^{-2} with a 95% confidence interval ranging from 0.23 to 0.50 µg m^{-2} (Figure 4). The modeled flux was one-third of the measured flux. The average RM dry deposition velocities of Hg(OH)$_2$, HgBr$_2$/HgCl$_2$, HgN$_2$O$_6$, HgSO$_4$, MeHg were very similar and differed by less than 5% during each sampling week (Table S6). The dominant RM compounds HgBr$_2$/HgCl$_2$ and

391   HgN$_2$O$_6$ both exhibited a mean deposition velocity of 0.28 ± 0.10 cm s^{-1} over the course of the

392   campaign. The weekly mean RM deposition velocities ranged from 0.12 cm s^{-1} (week 15) to 0.48 cm s^{-1}

393   (week 10). The mean deposition velocity of all RM compounds was 0.32 ± 0.09 cm s^{-1} when the area

394   around Zeppelin was covered by snow, and 0.21 ± 0.08 cm s^{-1} during the last five weeks of

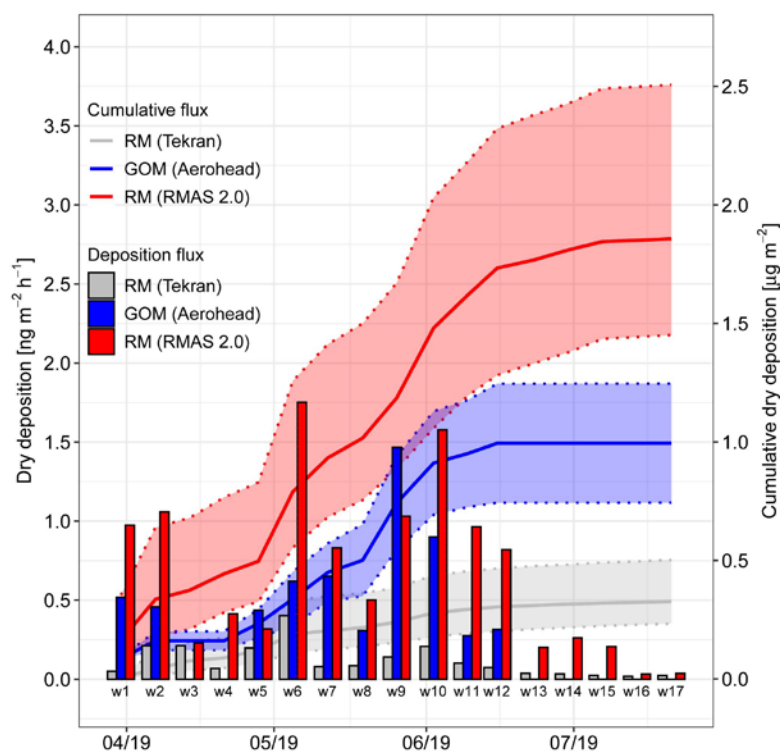395   measurements when snowmelt had occurred (June 17, 2019).

Figure 4: Measured GOM and modeled RM dry deposition for the entire sampling period. Weekly GOM dry deposition calculated based on the Aerohead system (measured) and RM dry deposition estimated based on the Tekran® and RMAS systems using RM compound-specific dry deposition velocities (modeled). The cumulative flux over the entire sampling campaign (lines) and associated uncertainties (shaded area, 95% confidence interval) are given.

396   The modeled cumulative dry deposition based on RM$_{CEM}$ was 1.86 µg m^{-2} with a 95% confidence

397   interval ranging from 1.45 to 2.50 µg m^{-2} (Figure 4). Thus, RM dry deposition was 5.6 times larger

398   compared to estimates using Tekran® data (Table S7). The discrepancy between the measured

399   (Aerohead) and the modeled (RMAS) cumulative dry deposition, a factor of 1.9, was due to the

400   Aerohead sampling GOM, while PBM adsorbs negligibly to the down-facing surrogate surface due to

401   gravity[22,34-36,79-81]. The inconsistency during weeks 1, 2, and 6 could accordingly be explained by

402   elevated concentrations of particulate matter (PM$_{total}$), indicating that PBM dominated RM dry

403   deposition during these weeks (Figure S2). The inconsistency in weeks 10, 11 and 12, however, was

404   likely associated with elevated RM dry deposition velocities (0.47 cm s^{-1}), given the low PBM

405   concentrations, as compared to the other weeks (0.25 cm s^{-1}) that are not reproduced by the Aerohead

406   measurements. It is likely that Hg–N RM compounds were advected on particles, especially during

407   weeks 1 and 6 when the absolute amount of Hg–N RM compounds was elevated (Figure 2a). During

408   the entire campaign, though, the ammonium (NH$_4^+$) and nitrate (NO$_3^-$) aerosol concentration was at

409   least three orders of magnitude higher compared to the concentrations of Hg–N compounds. This

indicates that RM production and transformation of Hg–N compounds was not directly linked to advection of particulate nitrogen compounds, which is consistent with a predominant gas-phase oxidation of RM precursor by NO_2 in the FT[64].

3.6 Implications

Arctic RM concentrations analyzed on CEM and PES were higher than Tekran® RM during all weeks of measurements. That the Tekran® system significantly underestimated RM concentrations in the Arctic was surprising since one would expect that most of the RM would be Br and Cl compounds and given the efficiency of the denuder the KCl denuder it should be 1.2 to 1.3 times lower as demonstrated in Huang et al.,[21]. But Huang et al. [21]'s experiments were done in clean air whereas the measurements in the Arctic were of ambient air, indicating the impact of some aspect atmospheric chemistry (e.g. O_3) on retention of GOM compounds.The difference between RM concentrations was large during the AMDE season (mainly April and May) and became small when the RM concentrations decreased in the summer. In general, RM_{TK} showed a significant, but not strong, correlation ($r^2 < 0.6$) with RM_{CEM} and RM_{PES}. Bias in denuder-based Tekran® quantification of GOM could not be corrected, as was suggested for the Pic du Midi high-altidute site in the Pyrenees, France[25]. The bias in Arctic RM concentration measurements between manual and automated methods must be addressed not only during AMDEs but with multi-seasonal sampling campaigns at sites such as Alert in Canada, where Tekran® systems are also operated year-round.

RM compound-specific deposition velocity estimates provide the way for more accurate RM dry deposition estimates. However, as stated in Gustin et al.[63], the determination of RM compounds could be improved by: 1) using a new thermal desorption surface, because the nylon membranes underestimate RM concentrations (by 50% in this study); and 2) identifying the exact chemistry of RM compounds by developing a mass spectrometry method.

The RM dry deposition model revealed higher fluxes when using the RMAS data compared to Tekran® data, suggesting a 5.6 times larger input of RM to Arctic ecosystems. In the Ny-Ålesund area, RM dry deposition (1.9 µg m^{-2} from March 27 to July 24, 2019) was the dominant Hg deposition pathway, exceeding mean annual wet deposition ranging from 0.8 to 1.7 µg m^{-2} yr^{-1} measured between 2012 and 2015[82].

If we accept the assumption that dry deposition measurements made by the Aerohead system are accurate for GOM and measurements performed with RMAS are accurate for RM, our results demonstrate that RM bound to particles constituted 46% of the deposited Hg; this also assumes that RM dry deposition occurs homogeneously and independently of different boundary layer conditions at Zeppelin. In fact, large particles > $PM_{2.5}$ (not analyzed by the Tekran®) contributed 70% to the total PM concentration (Figure S2). This indicates that a dominant portion of the RM was associated with large particles (> $PM_{2.5}$), likely marine aerosols. Our study showed that RM dry deposition estimates

during the 2019 AMDE season at Zeppelin, and potentially elsewhere in the Arctic, were likely higher than previously assumed and reported. This has implications for the amount of Hg cycling between the atmosphere and Arctic ecosystems.

Associated content (Supporting Information)

The Supporting Information (SI) is available free of charge on the ACS publication website. The SI is structured in six different sections (S1 – S6). We provide details on automated (S1) and manual (S2) RM sampling and analysis as well as an overview of the measured RM concentrations (S3). The thermal desorption procedure is described and profiles displayed (S4). Back trajectory modeling is detailed in S5 and supplementary information about dry deposition modeling is given in S6.

Author information (corresponding author)

Stefan Osterwalder - Institute of Agricultural Sciences, ETH Zurich, Universitätsstrasse 2, 8092 Zurich, Switzerland; orcid.org/0000-0001-8775-0813; Phone: +41 76 477 35 89; Email: stefan.osterwalder@usys.ethz.ch

Data availability

RM concentration data are given in the Supporting Information. A detailed model description is provided in https://github.com/JiaoyanHuang/Dry_Depo_multi_res_model. Raw data on thermal desorption and peak deconvolution procedures or from back trajectory modeling are available on request.

References

(1) AMAP Assessment 2011: Mercury in the Arctic., Arctic Monitoring and Assessment Programme (AMAP), Oslo, Norway., **2011**.

(2) Douglas, T.A., Loseto, L.L., Macdonald, R.W., Outridge, P., Dommergue, A., Poulain, A., Amyot, M., Barkay, T., Berg, T., Chételat, J., Constant, P., Evans, M., Ferrari, C., Gantner, N., Johnson, M.S., Kirk, J., Kroer, N., Larose, C., Lean, D., Nielsen, T.G., Poissant, L., Rognerud, S., Skov, H., Sørensen, S., Wang, F., Wilson, S. Zdanowicz, C.M. The fate of mercury in Arctic terrestrial and aquatic ecosystems, a review. *Environ. Chem.* **2012**, 9, 321-355. http://dx.doi.org/10.1071/EN11140

(3) UNEP Minamata Convention on Mercury: Text and Annexes. UNEP Chemicals Branch, Geneva, Switzerland, **2013**. http://www.mercuryconvention.org (last access: 12. April 2021).

(4) Soerensen, A.L., Jacob, D.J., Schartup, A.T., Fisher, J.A., Lehnherr, I., Louis, V.L.S., Heimbürger, L.-E., Sonke, J.E., Krabbenhoft, D.P., Sunderland, E.M. A mass budget for mercury and methylmercury in the Arctic Ocean. *Glob. Biogeochem. Cycles* **2016**, 30, 560–575. https://doi.org/10.1002/2015GB005280

(5) Dastoor, A.P. and Durnford, D.A. Arctic Ocean: Is It a Sink or a Source of Atmospheric Mercury? *Environ. Sci. Technol.* **2014**, 48, 1707-1717. https://doi.org/10.1021/es404473e

(6) Schroeder, W.H., Anlauf, K.G., Barrie, L.A., Lu, J.Y., Steffen, A., Schneeberger, D.R., Berg, T. Arctic springtime depletion of mercury. *Nature* **1998**, 394, 331–332. https://doi.org/10.1038/28530

(7) Ariya, P.A., Dastroor, A.P., Amyot, M., Schroeder, W.H., Barrie, L., Anlauf, K., Raofie, F., Ryzhkov, A., Davignon, D., Lalonde, J., Steffen, A. The Arctic: a sink for mercury. *Tellus B: Chemical and Physical Meteorology* **2004**, 56, 397–403. https://doi.org/10.3402/tellusb.v56i5.16458

(8) Skov, H., Christensen, J. H., Goodsite, M. E., Heidam, N. Z., Jensen, B., Wåhlin, P., Geernaert, G. Fate of elemental mercury in the arctic during atmospheric mercury depletion episodes and the load of atmospheric mercury to the arctic. *Environ. Sci. Technol.* **2004**, 38, 2373–2382. https://doi.org/10.1021/es030080h

(9) Lindberg, S. E., Brooks, S., Lin, C.-J., Scott, K. J., Landis, M. S., Stevens, R. K., Goodsite,M. E., Richter, A. Dynamic oxidation of gaseous mercury in the arctic troposphere at polar sunrise. *Environ. Sci. Technol.* **2002**, 36, 1245–1256. https://doi.org/10.1021/es0111941

(10) Steffen, A., T. Douglas, M. Amyot, P. Ariya, K. Aspmo, T. Berg, J. Bottenheim, S. Brooks, F. Cobbett, A. Dastoor, A. Dommergue, R. Ebinghaus, C. Ferrari, K. Gardfeldt, M.E. Goodsite, D. Lean, A.J. Poulain, C. Scherz, H. Skov, J. Sommar, Temme, C. A synthesis of atmospheric mercury depletion event chemistry in the atmosphere and snow. *Atmos. Chem. and Phys*. **2008**, 8, 1445–1482. https://doi.org/10.5194/acp-8-1445-2008

(11) Wang, S., McNamara, S.M., Moore, C.W., Obrist, D., Steffen, A., Shepson, P.B., Staebler, R.M., Raso, A.R.W., Pratt, K.A. Direct detection of atmospheric atomic bromine leading to mercury and ozone depletion. *PNAS* **2019**, 116, 14479–14484. https://doi.org/10.1073/pnas.1900613116

(12) Obrist, D., Agnan, Y., Jiskra, M., Olson, C.L., Colegrove, D.P., Hueber, J., Moore, C.W., Sonke,

J.E., Helmig, D. Tundra uptake of atmospheric elemental mercury drives Arctic mercury pollution. *Nature* **2017**, 547, 201–204. https://www.nature.com/articles/nature22997

(13)　Dommergue, A., Larose, C., Faïn, X., Clarisse, O., Foucher, D., Hintelmann, H., Schneider, D., Ferrari, C.P. Deposition of Mercury Species in the Ny-Ålesund Area (79°N) and Their Transfer during Snowmelt. *Environ. Sci. Technol.* **2010**, 44, 901–907. https://doi.org/10.1021/es902579m

(14)　Steffen, A., Bottenheim, J., Cole, A., Ebinghaus, R., Lawson, G., Leaitch, W. R. Atmospheric mercury speciation and mercury in snow over time at Alert, Canada, *Atmos. Chem. Phys.* **2014**, 14, 2219–2231. https://doi:10.5194/acp-14-2219-2014

(15)　Kamp, J., Skov, H., Jensen, B., Sørensen, L.L. Fluxes of gaseous elemental mercury (GEM) in the High Arctic during atmospheric mercury depletion events (AMDEs). *Atmos. Chem. Phys.* **2018**, 18, 6923–6938. https://doi.org/10.5194/acp-18-6923-2018

(16)　Jiskra, M., Sonke, J.E., Agnan, Y., Helmig, D., Obrist, D. Insights from mercury stable isotopes on terrestrial–atmosphere exchange of Hg(0) in the Arctic tundra. *Biogeosciences* **2019**, 16, 4051–4064. https://doi.org/10.5194/bg-16-4051-2019

(17)　Gustin, M. S.; Huang, J.; Miller, M. B.; Peterson, C.; Jaffe, D. A.; Ambrose, J.; Finley, B. D.; Lyman, S. N.; Call, K.; Talbot, R.; Feddersen, D.; Mao, H.; Lindberg, S. E. Do We Understand What the Mercury Speciation Instruments Are Actually Measuring? Results of RAMIX. *Environ. Sci. Technol.* **2013**, 47, 7295−7306.

(18)　Gustin, M.S., Amos, H.M., Huang, J., Miller, M.B., Heidecorn, K. Measuring and modeling mercury in the atmosphere: a critical review. *Atmos. Chem. Phys.* **2015**, 15, 5697–5713. https://doi.org/10.5194/acp-15-5697-2015

(19)　Gustin, M.S., Dunham-Cheatham, S.M., Zhang, L. Comparison of 4 Methods for Measurement of Reactive, Gaseous Oxidized, and Particulate Bound Mercury. *Environ. Sci. Technol.* **2019**, 53, 14489–14495. https://doi.org/10.1021/acs.est.9b04648

(20)　Gustin, M.S., Dunham-Cheatham, S.M., Zhang, L., Lyman, S., Choma, N., Castro, M. Use of Membranes and Detailed HYSPLIT Analyses to Understand Atmospheric Particulate, Gaseous Oxidized, and Reactive Mercury Chemistry. *Environ. Sci. Technol.* **2021a**, 55, 893–901. https://doi.org/10.1021/acs.est.0c07876

(21)　Huang, J.; Miller, M. B.; Weiss-Penzias, P.; Gustin, M. S. Comparison of Gaseous Oxidized Hg Measured by KCl-Coated Denuders, and Nylon and Cation Exchange Membranes. *Environ. Sci. Technol.* **2013**, 47, 7307−7316. https://doi.org/10.1021/es4012349

(22)　Huang, J., Miller, M.B., Edgerton, E., Gustin, M.S. Use of criteria pollutants, active and passive mercury sampling, and receptor modeling to understand the chemical forms of gaseous oxidized mercury in Florida. *Atmos. Chem. Phys. Discuss.* **2015**, 12069–12105. https://doi.org/10.5194/acpd-15-12069-2015

(23)　McClure, C.D., Jaffe, D.A., Edgerton, E.S. Evaluation of the KCl Denuder Method for Gaseous Oxidized Mercury using HgBr2 at an In-Service AMNet Site. *Environ. Sci. Technol.* **2014**, 48,

552 11437–11444. https://doi.org/10.1021/es502545k

553 (24) Luippold, A., Gustin, M.S., Dunham-Cheatham, S.M., Castro, M., Luke, W., Lyman, S., Zhang, L.
554   Use of Multiple Lines of Evidence to Understand Reactive Mercury Concentrations and Chemistry in
555   Hawai'i, Nevada, Maryland, and Utah, USA. *Environ. Sci. Technol.* **2020a**, 54, 7922–7931.
556   https://doi.org/10.1021/acs.est.0c02283

557 (25) Maruszczak, N., Sonke, J.E., Fu, X., Jiskra, M. Tropospheric GOM at the Pic du Midi Observatory –
558   correcting bias in denuder based observations. *Environ. Sci. Technol.* **2017**, 51, 863–869.
559   https://doi.org/10.1021/acs.est.6b04999

560 (26) Lynam, M.M., and Keeler, G.J. Artifacts associated with the measurement of particulate mercury in
561   an urban environment: The influence of elevated ozone concentrations. *Atmospheric Environ.* **2005**,
562   39, 3081–3088. http://dx.doi.org/10.1016/j.atmosenv.2005.01.036

563 (27) Malcolm, E.G., and Keeler, G.J.: Evidence for a sampling artifact for particulate-phase mercury in
564   the marine atmosphere, *Atmospheric Environ.* **2007**, 41, 3352–3359.
565   https://doi.org/10.1016/j.atmosenv.2006.12.024

566 (28) Rutter, A.P., Hanford, K.L., Zwers, J.T., Perillo-Nicholas, A.L. Evaluation of an offline method for
567   the analysis of atmospheric reactive gaseous mercury and particulate mercury. *J. Air Waste Manag.*
568   *Assoc.* **2008**, 58, 377–383. https://doi.org/10.3155/1047-3289.58.3.377

569 (29) Kos, G., Ryzhkov, A., Dastoor, A., Narayan, J., Steffen, A., Ariya, P. A., Zhang, L. Evaluation of
570   discrepancy between measured and modelled oxidized mercury species, *Atmos. Chem. Phys.* **2013**,
571   13, 4839–4863. https://doi.org/10.5194/acp-13-4839-2013

572 (30) Talbot, R., Mao, H., Feddersen, D., Smith, M., Kim, S.Y., Sive, B., Haase, K., Ambrose, J., Zhou,
573   Y., Russo, R. Comparison of Particulate Mercury Measured with Manual and Automated Methods.
574   *Atmosphere* **2011**, 2, 1–20. https://doi.org/10.3390/atmos2010001

575 (31) Feddersen, D.M., Talbot, R., Mao, H., Sive, B.C. Size distribution of particulate mercury in marine
576   and coastal atmospheres. *Atmos. Chem. Phys.* **2012**, 12, 10899–10909. https://doi.org/10.5194/acp-
577   12-10899-2012

578 (32) Luippold, A., Gustin, M.S., Dunham-Cheatham, S.M., Zhang, L. Improvement of quantification and
579   identification of atmospheric reactive mercury. *Atmospheric Environ*. **2020b**, 224, 117307.
580   https://doi.org/10.1016/j.atmosenv.2020.117307

581 (33) Lyman, S.N., Gustin, M.S., Prestbo, E.M., Marsik, F.J. Estimation of Dry Deposition of Atmospheric
582   Mercury in Nevada by Direct and Indirect Methods. *Environ. Sci. Technol.* **2007**, 41, 1970–1976.
583   https://doi.org/10.1021/es062323m

584 (34) Lyman, S.N., Gustin, M.S., Prestbo, E.M., Kilner, P.I., Edgerton, E., Hartsell, B. Testing and
585   Application of Surrogate Surfaces for Understanding Potential Gaseous Oxidized Mercury Dry
586   Deposition. *Environ. Sci. Technol.* **2009**, 43, 6235–6241. https://doi.org/10.1021/es901192e

587 (35) Gustin, M.S, Weiss-Penzias, P.S., Peterson, C. Investigating sources of gaseous oxidized mercury in
588   dry deposition at three sites across Florida, USA. *Atmos. Chem. Phys.* **2012**, 12, 9201–9219.

589   https://doi.org/10.5194/acp-12-9201-2012

590   (36)   Huang, J., Miller, M.B., Edgerton, E., Gustin, M.S. Deciphering potential chemical compounds of
591   gaseous oxidized mercury in Florida, USA. *Atmos. Chem. Phys.* **2017**, 17, 1689−1698.
592   https://doi.org/10.5194/acp-17-1689-2017

593   (37)   Zhang, L., Brook, J.R., Vet, R. A revised parameterization for gaseous dry deposition in air-quality
594   models. *Atmos. Chem. Phys.* **2003**, 3, 2067–2082. https://doi.org/10.5194/acp-3-2067-2003

595   (38)   Berg, T., Bartnicki, J., Munthe, J., Lattila, H., Hrehoruk, J., Mazur, A. Atmospheric mercury species
596   in the European Arctic: Measurements and modelling. *Atmospheric Environ.* **2001**, 35, 2569–2582.
597   https://doi.org/10.1016/S1352-2310(00)00434-9

598   (39)   Berg, T., Pfaffhuber, K.A., Cole, A.S., Engelsen, O., Steffen, A.. Ten-year trends in atmospheric
599   mercury concentrations, meteorological effects and climate variables at Zeppelin, Ny-Ålesund.
600   *Atmos. Chem. Phys.* **2013**, 13, 6575–6586. https://doi.org/10.5194/acp-13-6575-2013

601   (40)   Berg, T., Sekkesæter, S., Steinnes, E., Valdal, A.-K., Wibetoe, G. Springtime depletion of mercury in
602   the European Arctic as observed at Svalbard. *Sci. Total Environ.* **2003**, Pathways and processes of
603   mercury in the environment. Selected papers presented at the sixth International Conference on
604   Mercury as Global Pollutant, Minamata, Japan, Oct. 15-19, 2001 304, 43–51.
605   https://doi.org/10.1016/S0048-9697(02)00555-7

606   (41)   Aspmo, K., Gauchard, P.-A., Steffen, A., Temme, C., Berg, T., Bahlmann, E., Banic, C.,
607   Dommergue, A., Ebinghaus, R., Ferrari, C., Pirrone, N., Sprovieri, F., Wibetoe, G. Measurements of
608   atmospheric mercury species during an international study of mercury depletion events at Ny-
609   Ålesund, Svalbard, spring 2003. How reproducible are our present methods? *Atmospheric Environ.*
610   **2005**, 39, 7607–7619. https://doi.org/10.1016/j.atmosenv.2005.07.065

611   (42)   Gauchard, P.-A., Aspmo, K., Temme, C., Steffen, A., Ferrari, C., Berg, T., Ström, J., Kaleschke, L.,
612   Dommergue, A., Bahlmann, E., Magand, O., Planchon, F., Ebinghaus, R., Banic, C., Nagorski, S.,
613   Baussand, P., Boutron, C. Study of the origin of atmospheric mercury depletion events recorded in
614   Ny-Ålesund, Svalbard, spring 2003. *Atmospheric Environ.* **2005**, 39, 7620–7632.
615   https://doi.org/10.1016/j.atmosenv.2005.08.010

616   (43)   Sprovieri, F., Pirrone, N., Landis, M.S., Stevens, R.K. Oxidation of Gaseous Elemental Mercury to
617   Gaseous Divalent Mercury during 2003 Polar Sunrise at Ny-Ålesund. *Environ. Sci. Technol.* **2005a**,
618   39, 9156–9165, https:// doi.org/10.1021/es050965o

619   (44)   Sprovieri, F., Pirrone, N., Landis, M.S., Stevens, R.K. Atmospheric mercury behavior at different
620   altitudes at Ny-Ålesund during Spring 2003. *Atmospheric Environ.* **2005b**, 39, 7646–7656.
621   https://doi.org/10.1016/j.atmosenv.2005.08.001

622   (45)   Sommar, J., Wängberg, I., Berg, T., Gårdfeldt, K., Munthe, J., Richter, A., Urba, A., Wittrock, F.,
623   Schroeder, W. H. Circumpolar transport and air-surface exchange of atmospheric mercury at Ny-
624   Ålesund (79° N), Svalbard, spring 2002. *Atmos. Chem. Phys.* **2007**, 7, 151–166, doi:10.5194/acp-7-
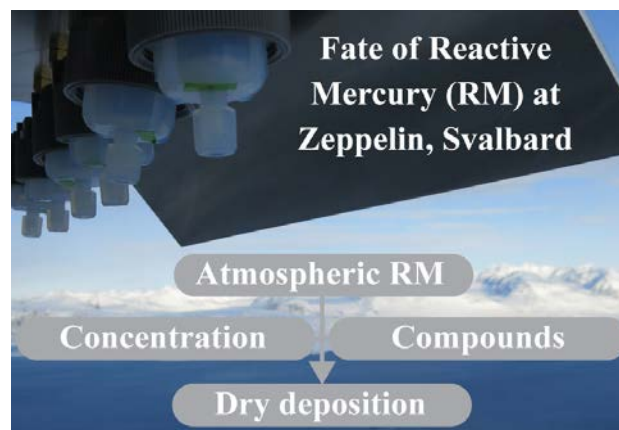625   151-2007

626　(46)　Ferrari, C.P., Padova, C., Faïn, X., Gauchard, P.-A., Dommergue, A., Aspmo, K., Berg, T., Cairns,
627　　　　W., Barbante, C., Cescon, P., Kaleschke, L., Richter, A., Wittrock, F., Boutron, C. Atmospheric
628　　　　mercury depletion event study in Ny-Alesund (Svalbard) in spring 2005. Deposition and
629　　　　transformation of Hg in surface snow during springtime. *Sci. Total Environ.* **2008**, 397, 167–177.
630　　　　https://doi.org/10.1016/j.scitotenv.2008.01.064

631　(47)　Steen, A.O., Berg, T., Dastoor, A.P., Durnford, D.A., Engelsen, O., Hole, L.R., Pfaffhuber, K.A.
632　　　　Natural and anthropogenic atmospheric mercury in the European Arctic: a fractionation study. *Atmos.*
633　　　　*Chem. Phys.* **2011**, 11, 6273–6284. https://doi.org/10.5194/acp-11-6273-2011

634　(48)　Angot, H., Dastoor, A., De Simone, F., Gårdfeldt, K., Gencarelli, C.N., Hedgecock, I.M., Langer, S.,
635　　　　Magand, O., Mastromonaco, M.N., Nordstrøm, C., Pfaffhuber, K.A., Pirrone, N., Ryjkov, A., Selin,
636　　　　N.E., Skov, H., Song, S., Sprovieri, F., Steffen, A., Toyota, K., Travnikov, O., Yang, X.,
637　　　　Dommergue, A. Chemical cycling and deposition of atmospheric mercury in polar regions: review of
638　　　　recent measurements and comparison with models. *Atmos. Chem. Phys.* **2016**, 16, 10735–10763.
639　　　　https://doi.org/10.5194/acp-16-10735-2016

640　(49)　Landis, M.S., Stevens, R.K., Schaedlich, F., Prestbo, E.M. Development and Characterization of an
641　　　　Annular Denuder Methodology for the Measurement of Divalent Inorganic Reactive Gaseous
642　　　　Mercury in Ambient Air. *Environ. Sci. Technol.* **2002**, 36, 3000–3009.
643　　　　https://doi.org/10.1021/es015887t

644　(50)　Steffen, A., Scherz, T., Olson, M., Gay, D., Blanchard, P. A comparison of data quality control
645　　　　protocols for atmospheric mercury speciation measurements. *J. Environ. Monit.* **2012**, 14, 752–765.
646　　　　https://doi.org/10.1039/C2EM10735J

647　(51)　D'Amore, F., Bencardino, M., Cinnirella, S., Sprovieri, F., Pirrone, N. Data quality through a web-
648　　　　based QA/QC system: implementation for atmospheric mercury data from the global mercury
649　　　　observation system. *Environ. Sci.: Processes Impacts* **2015**, 17, 1482–1491.
650　　　　https://doi.org/10.1039/C5EM00205B

651　(52)　Enrico, M., Le Roux, G., Marusczak, N., Heimburger, L.-E., Claustres, A., Fu, X., Sun, R., Sonke,
652　　　　J.E. Atmospheric mercury transfer to peat bogs dominated by gaseous elemental mercury dry
653　　　　deposition. *Environ. Sci. Technol.* **2016**, 50, 2405–2412. https://doi.org/10.1021/acs.est.5b06058

654　(53)　Dunham-Cheatham, S.M., Lyman, S., Gustin, M.S. Evaluation of sorption surface materials for
655　　　　reactive mercury compounds. *Atmospheric Environ.* 2020, 242, 117836.
656　　　　https://doi.org/10.1016/j.atmosenv.2020.117836

657　(54)　Miller, M.B., Dunham-Cheatham, S.M., Gustin, M.S., Edwards, G.C. Evaluation of cation exchange
658　　　　membrane performance under exposure to high Hg0 and HgBr2 concentrations. *Atmos. Meas. Tech.*
659　　　　**2019**, 12, 1207–1217. https://doi.org/10.5194/amt-12-1207-2019

660　(55)　Biester, H. and Scholz, C. Determination of Mercury Binding Forms in Contaminated Soils: Mercury
661　　　　Pyrolysis versus Sequential Extractions. *Environ. Sci. Technol.* 1996, 31, 233-239.
662　　　　https://doi.org/10.1021/es960369h

663　(56)　Stein, A.F., Draxler, R.R., Rolph, G.D., Stunder, B.J.B., Cohen, M.D., Ngan, F. NOAA's HYSPLIT

664   Atmospheric Transport and Dispersion Modeling System. *Bull. Ame. Meteorol. Soc.* **2015**, 96, 2059–
665   2077. https://doi.org/10.1175/BAMS-D-14-00110.1

666 (57) Hersbach, H., Bell, B., Berrisford, P., Hirahara, S., Horányi, A., Muñoz-Sabater, J., Nicolas, J.,
667   Peubey, C., Radu, R., Schepers, D., Simmons, A., Soci, C., Abdalla, S., Abellan, X., Balsamo, G.,
668   Bechtold, P., Biavati, G., Bidlot, J., Bonavita, M., Chiara, G.D., Dahlgren, P., Dee, D., Diamantakis,
669   M., Dragani, R., Flemming, J., Forbes, R., Fuentes, M., Geer, A., Haimberger, L., Healy, S., Hogan,
670   R.J., Hólm, E., Janisková, M., Keeley, S., Laloyaux, P., Lopez, P., Lupu, C., Radnoti, G., Rosnay, P.
671   de, Rozum, I., Vamborg, F., Villaume, S., Thépaut, J.-N. The ERA5 global reanalysis. *Q. J. R.*
672   *Meteorol. Soc.* **2020**, 146, 1999–2049. https://doi.org/10.1002/qj.3803

673 (58) Boike, J., Juszak, I., Lange, S., Chadburn, S., Burke, E.J., Overduin, P.P., Roth, K., Ippisch, O.,
674   Bornemann, N., Stern, L., Gouttevin, I., Hauber, E., Westermann, S. Measurements in soil and air at
675   Bayelva Station. Supplement to: Boike, J et al. (2018): A 20-year record (1998-2017) of permafrost,
676   active layer and meteorological conditions at a high Arctic permafrost research site (Bayelva,
677   Spitsbergen). *Earth Syst. Sci. Data*, **2017**, 10, 355-390, https://doi.org/10.5194/essd-10-355-2018.

678 (59) EMEP. Manual for sampling and chemical analysis, Norwegian Institute for Air Research, Kjeller,
679   EMEP Report 1/95 (Last rev. 2001), https://projects.nilu.no/ccc/manual/index.html (last access: 12.
680   April 2021)

681 (60) Hirdman, D., Aspmo, K., Burkhart, J.F., Eckhardt, S., Sodemann, H., Stohl, A. Transport of mercury
682   in the Arctic atmosphere: Evidence for a spring-time net sink and summer-time source. *Geophys.*
683   *Res. Lett.* **2009**, 36. https://doi.org/10.1029/2009GL038345

684 (61) Fisher, J.A., Jacob, D.J., Soerensen, A.L., Amos, H.M., Steffen, A., Sunderland, E.M. Riverine
685   source of Arctic Ocean mercury inferred from atmospheric observations. *Nat. Geosci.* **2012**, 5, 499–
686   504. https://doi.org/10.1038/ngeo1478

687 (62) Sonke, J.E., Teisserenc, R., Heimbürger-Boavida, L.-E., Petrova, M.V., Marusczak, N., Dantec, T.L.,
688   Chupakov, A.V., Li, C., Thackray, C.P., Sunderland, E.M., Tananaev, N., Pokrovsky, O.S. Eurasian
689   river spring flood observations support net Arctic Ocean mercury export to the atmosphere and
690   Atlantic Ocean. *PNAS* **2018**, 115, E11586–E11594. https://doi.org/10.1073/pnas.1811957115

691 (63) Gustin, M.S., Dunham-Cheatham, S.M., Huang, J., Lindberg, S., Lyman, S.N. Development of an
692   Understanding of Reactive Mercury in Ambient Air: A Review. *Atmosphere* **2021b**, 12, 73.
693   https://doi.org/10.3390/atmos12010073

694 (64) Horowitz, H.M., Jacob, D.J., Zhang, Y., Dibble, T.S., Slemr, F., Amos, H.M., Schmidt, J.A., Corbitt,
695   E.S., Marais, E.A., Sunderland, E.M. A new mechanism for atmospheric mercury redox chemistry:
696   implications for the global mercury budget. *Atmos. Chem. Phys.* **2017**, 17, 6353–6371.
697   https://doi.org/10.5194/acp-17-6353-2017

698 (65) Peleg, M., Tas, E., Obrist, D., Matveev, V., Moore, C., Gabay, M., Luria, M. Observational Evidence
699   for Involvement of Nitrate Radicals in Nighttime Oxidation of Mercury. *Environ. Sci. Technol.* **2015**,
700   49, 14008–14018. https://doi.org/10.1021/acs.est.5b03894

701 (66) Jiao, Y. and Dibble, T.S. First kinetic study of the atmospherically important reactions BrHg˙ + NO2

and BrHg˙ + HOO. *Phys. Chem. Chem. Phys.* **2017**, 19, 1826–1838. https://doi.org/10.1039/C6CP06276H

(67) Lam, K.T., Wilhelmsen, C.J., Schwid, A.C., Jiao, Y., Dibble, T.S. Computational Study on the Photolysis of BrHgONO and the Reactions of BrHgO• with CH4, C2H6, NO, and NO2: Implications for Formation of Hg(II) Compounds in the Atmosphere. *J. Phys. Chem. A.* **2019**, 123, 1637–1647. https://doi.org/10.1021/acs.jpca.8b11216

(68) Dibble, T.S., Zelie, M.J., Mao, H. Thermodynamics of reactions of ClHg and BrHg radicals with atmospherically abundant free radicals. *Atmos. Chem. Phys.* **2012**, 12, 10271–10279. https://doi.org/10.5194/acp-12-10271-2012

(69) Toyota, K., McConnell, J.C., Lupu, A., Neary, L., McLinden, C.A., Richter, A., Kwok, R., Semeniuk, K., Kaminski, J.W., Gong, S.-L., Jarosz, J., Chipperfield, M.P., Sioris, C.E., 2011. Analysis of reactive bromine production and ozone depletion in the Arctic boundary layer using 3-D simulations with GEM-AQ: inference from synoptic-scale patterns. Atmospheric Chemistry and Physics 11, 3949–3979. https://doi.org/10.5194/acp-11-3949-2011

(70) Yang, X., Pyle, J.A., Cox, R.A., 2008. Sea salt aerosol production and bromine release: Role of snow on sea ice. Geophysical Research Letters 35. https://doi.org/10.1029/2008GL034536

(71) Huang, J., Jaeglé, L., Chen, Q., Alexander, B., Sherwen, T., Evans, M. J., Theys, N., and Choi, S., 2020. Evaluating the impact of blowing snow sea salt aerosol on springtime BrO and O3 in the Arctic, Atmos. Chem. Phys., 20, 7335–7358,https://doi.org/10.5194/acp-20-7335-2020.

(72) Simpson, W.R., Brown, S.S., Saiz-Lopez, A., Thornton, J.A., von Glasow, R. Tropospheric Halogen Chemistry: Sources, Cycling, and Impacts. *Chem. Rev.* **2015**, 115, 4035–4062. https://doi.org/10.1021/cr5006638

(73) Simpson, W.R., Glasow, R. von, Riedel, K., Anderson, P., Ariya, P., Bottenheim, J., Burrows, J., Carpenter, L.J., Friess, U., Goodsite, M.E., Heard, D., Hutterli, M., Jacobi, H.W., Kaleschke, L., Neff, B., Plane, J., Platt, U., Richter, A., Roscoe, H., Sander, R., Shepson, P., Sodeau, J., Steffen, A., Wagner, T., Wolff, E. Halogens and their role in polar boundary-layer ozone depletion. *Atmos. Chem. Phys.* **2007**, 7, 4375–4418. https://doi.org/10.5194/acp-7-4375-2007

(74) Abbatt, J.P.D., Thomas, J.L., Abrahamsson, K., Boxe, C., Granfors, A., Jones, A.E., King, M.D., Saiz-Lopez, A., Shepson, P.B., Sodeau, J., Toohey, D.W., Toubin, C., von Glasow, R., Wren, S.N., Yang, X. Halogen activation via interactions with environmental ice and snow in the polar lower troposphere and other regions. *Atmos. Chem. Phys.* **2012**, 12, 6237–6271. https://doi.org/10.5194/acp-12-6237-2012

(75) Foster, K.L., Plastridge, R.A., Bottenheim, J.W., Shepson, P.B., Finlayson-Pitts, B.J., Spicer, C.W. The Role of Br2 and BrCl in Surface Ozone Destruction at Polar Sunrise. *Science* **2001**, 291, 471–474. https://doi.org/10.1126/science.291.5503.471

(76) Liao, J., Huey, L.G., Liu, Z., Tanner, D.J., Cantrell, C.A., Orlando, J.J., Flocke, F.M., Shepson, P.B., Weinheimer, A.J., Hall, S.R., Ullmann, K., Beine, H.J., Wang, Y., Ingall, E.D., Stephens, C.R., Hornbrook, R.S., Apel, E.C., Riemer, D., Fried, A., Mauldin, R.L., Smith, J.N., Staebler, R.M.,

740   Neuman, J.A., Nowak, J.B. High levels of molecular chlorine in the Arctic atmosphere. *Nat. Geosci.*
741   **2014**, 7, 91–94. https://doi.org/10.1038/ngeo2046

742   (77)   Zhang, L. and Jaffe, D.A. Trends and sources of ozone and sub-micron aerosols at the Mt. Bachelor
743   Observatory (MBO) during 2004-2015. *Atmospheric Environ.* **2017**, 165, 143–154.
744   https://doi.org/10.1016/j.atmosenv.2017.06.042

745   (78)   Pal, B. and Ariya, P.A. Studies of ozone initiated reactions of gaseous mercury: kinetics, product
746   studies, and atmospheric implications. *Phys. Chem. Chem. Phys.* 2004, 6, 572–579.
747   https://doi.org/10.1039/B311150D

748   (79)   Lyman, S. N., Gustin, M. S., Prestbo, E. M. A passive sampler for ambient gaseous oxidized mercury
749   concentrations. *Atmospheric Environ.* **2010**, 44, 246–252.
750   https://doi.org/10.1016/j.atmosenv.2009.10.008

751   (80)   Huang, J., Lyman, S.N., Hartman, J.S., Gustin, M.S. A review of passive sampling systems for
752   ambient air mercury measurements. *Environ. Sci. Process Impacts* **2014**, 16, 374–392.
753   https://doi.org/10.1039/c3em00501a

754   (81)   Huang, J. and Gustin, M.S. Uncertainties of Gaseous Oxidized Mercury Measurements Using KCl-
755   Coated Denuders, Cation-Exchange Membranes, and Nylon Membranes: Humidity Influences.
756   *Environ. Sci. Technol.* **2015**, 49, 6102–6108. https://doi.org/10.1021/acs.est.5b00098

757   (82)   Sprovieri, F., Pirrone, N., Bencardino, M., D'Amore, F., Angot, H., Barbante, C., Brunke, E.-G.,
758   Arcega-Cabrera, F., Cairns, W., Comero, S., Diéguez, M.D.C., Dommergue, A., Ebinghaus, R.,
759   Feng, X.B., Fu, X., Garcia, P.E., Gawlik, B.M., Hageström, U., Hansson, K., Horvat, M., Kotnik, J.,
760   Labuschagne, C., Magand, O., Martin, L., Mashyanov, N., Mkololo, T., Munthe, J., Obolkin, V.,
761   Ramirez Islas, M., Sena, F., Somerset, V., Spandow, P., Vardè, M., Walters, C., Wängberg, I.,
762   Weigelt, A., Yang, X., Zhang, H. Five-year records of mercury wet deposition flux at GMOS sites in
763   the Northern and Southern hemispheres. *Atmos. Chem. Phys.* **2017**, 17, 2689–2708.
764   https://doi.org/10.5194/acp-17-2689-2017

765

TOC